Preprint
UCRL-JC- 136297

Indirect-Drive Time Dependent Symmetry Diagnosis at NIF-Scale

O.L. Landen, D.K. Bradley, S.M. Pollaine, P.A. Amendt, S.G. Glendinning, L.J. Suter, R.E. Turner, R.J. Wallace, B.A. Hammel, N.D. Delamater, J. Wallace, G. Magelssen, P. Gobby

This article was submitted to First International Conference on Inertial Fusion Sciences and Applications, Bordeaux, France, September 12-17, 1999

U.S. Department of Energy
Lawrence Livermore National Laboratory

October 27, 1999

Indirect-Drive Time-Dependent Symmetry Diagnosis at NIF-Scale*

O.L. Landen[a], D.K. Bradley[a], S.M. Pollaine[a], P.A. Amendt[a], S.G. Glendinning[a], L.J. Suter[a], R.E. Turner[a], R.J. Wallace[a], B.A. Hammel[a], N.D. Delamater[b], J. Wallace[b], G. Magelssen[b], and P. Gobby[b]

[a]Lawrence Livermore National Laboratory, Livermore, CA, 94551
[b]Los Alamos National Laboratory, Los Alamos, NM, 87545

Abstract

The scaling to NIF of current techniques used to infer the time-dependent flux asymmetries for indirectly-driven capsules is reviewed. We calculate that the projected accuracy for detecting the lowest mode asymmetries by a variety of techniques now meet the requirements for symmetry tuning for ignition. The scaling to NIF has also motivated the implementation of new, more efficient and hence less perturbative backlighting techniques which have recently provided high quality symmetry data during validation tests at the Omega facility.

1. Introduction

The maximum tolerable asymmetry levels at capsules driven by cylindrical NIF ignition hohlraums can be decomposed into a Legendre expansion [1, 2]. For a peak drive temperature of 300 eV at NIF-scale, the tolerable levels are shown in *Fig. 1*: 10-20/τ(ns) % for the time-dependent P_2 averaged over any time interval τ, 1% for the time-integrated P_2, 0.5-1% for the time-integrated P_4, P_6 and P_8. Averaging over just the 10 ns foot of the NIF pulse, the tolerable asymmetry levels are 1-2% for modes P_2 through P_6 and 0.5-1% for mode P_8 [3]. The range in symmetry requirements reflects the fact that ignition also depends on the level of imbalances and inefficiencies on other laser and target parameters.

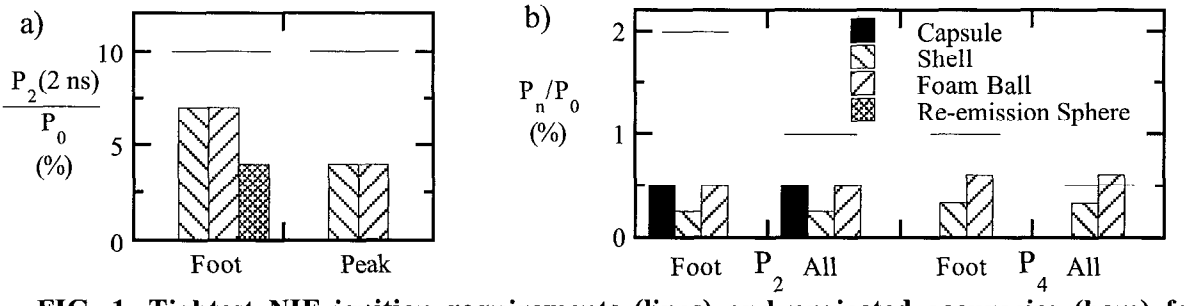

FIG. 1. Tightest NIF ignition requirements (lines) and projected accuracies (bars) for inferring low mode flux asymmetries from various asymmetry diagnosis techniques as a function of Legendre mode number P_n. a) P_2 averaged over any 2 ns interval. b) P_2 and P_4, averaged over foot of NIF ignition pulse and over all of pulse.

2. Time-Dependent Symmetry Measurement Techniques

The time-integrated asymmetry can be inferred from the distortions of imploded capsules viewed in self emission [4-8]; the scaling of this technique to NIF is dealt with in a companion paper [9]. Techniques for inferring the time-dependent flux asymmetries have included recording either the hohlraum wall emission profiles or sampling the capsule environment. For the former, both thermal x-ray [10] and hard x-ray imaging of the wall and spot emission [7, 11] has been used. For the latter, the ignition capsule is replaced by a variety of surrogate spheres designed to enhance the effects of and provide time-dependent

information on flux asymmetries. These latter x-ray techniques include measurements of re-emission patterns from non-imploding high Z spheres [12, 13], distortions of backlit shock-driven foam balls [14-16] and capsule shells [17]. We consider each surrogate sphere in turn.

2.1 Re-emission Sphere

For the high Z sphere, the local re-emission flux is used as a measure of the local incident flux [12, 13]. The re-emission technique is best suited to measurements during the earliest stages of the drive before ablative expansion of the sphere surface; later-time measurements have been demonstrated by overcoating the high-Z surface with a bleachable low Z layer which delays arrival of the radiation front and hence ablation of the high-Z surface. The accuracy on the measurement of the flux asymmetry is enhanced by choosing a re-emission photon energy hν that is many times the thermal temperature kT of the hohlraum drive. Specifically, it is easy to show that in the limit of Planckian sources, an n % incident flux asymmetry results in an n x (hν/4kT) % re-emission flux asymmetry. There is a practical limit however to the maximum usable hν as the re-emission flux falls off exponentially with photon energy. To date, with hν/4kT = 4 with T = 160 eV, a 15 % accuracy in extracting the lowest order re-emission asymmetry has been demonstrated, translating to a 4 % accuracy [13] in inferring an instantaneous P_2 asymmetry.

2.2 Backlit Foamball

For the foamball technique, ablation pressure asymmetries P_n are inferred from the distortions experienced by a shock-driven low density solid foam sphere [14, 15]. The pressure asymmetries produce spatial distortions in the shock and hence out-of-round edges to the foam ball which are recorded by radiography. Since the edge velocities follow shock velocities proportional to $\sqrt{(P/\rho)}$ [14], the lower the initial foam density $\rho\_$ the greater the difference in edge velocities v for a given flux asymmetry and the greater the perceived distortion after a given time interval. The limit on the minimum usable density is when the heat front becomes supersonic and a shock no longer forms. Such a regime occurs when the edge velocity reaches 1.5-2x the heated material sound speed c_s. For the typical mid Z (SiO_2) foam balls, this translates into maximum edge velocities of 100 (180) μm/ns for hohlraum drive temperatures of 100 (300) eV, respectively. The edge speed can be maximized for a given temperature by minimizing the foam density, with the minimum $\rho\_$ for $SiO_2 \sim T^2$ [14].

The spatial distortion, decomposed into Legendre moments a_n, are related to the running integral of the applied pressure asymmetries P_n (expressed as a fraction of the zeroth order pressure moment P_0) by:

$$a_n(\tau) = -1/2\int vP_n(t)dt, \; = \; -1/2a_0(\tau)P_n \qquad \text{(for constant } P_n\text{)} \qquad (1)$$

The reduction in sensitivity represented by the factor 1/2 arises from the square root dependence of shock velocity on pressure. The negative sign accounts for the fact that a larger local pressure leads to a dimple on the ball. Eq. (1) also shows that for a given measurement accuracy for a_n, the limit in accuracy in inferring P_n is only dependent on the maximum edge velocity $v \sim \sqrt{T}$. Hence, the inherent accuracy of the foam ball technique only depends on the drive temperature. Current simulated and demonstrated accuracy in recording for example an a_2 distortion is 1 μm [15].

2.3 Backlit Shells

For the backlit shell technique, ablation pressure asymmetries P_n are inferred from the distortions experienced during acceleration of a thin shell after shock transit. If we approximate the shell areal mass density as constant in time (i.e. the areal mass density

decrease through ablation is cancelled by the increase due to convergence), the shell distortion a_n is related to the fractional pressure asymmetry P_n after a time τ by:

$$a_n(\tau) = -a_0(\tau)\iint P_n P_0 dtdt' / \iint P_0 dtdt', \; = \; - a_0(\tau) P_n \quad \text{for constant } P_n \qquad (2)$$

Eq. (2) also assumes a constant shell thickness as the shell converges. If the shell thickens by x %, the distortion would also grow by an additional x %, the Bell-Plesset effect [18, 19].

3. Accuracy of Symmetry Techniques at NIF-Scale

Based on the simple analytic formulae presented in Section 2, the accuracy of the symmetry techniques for NIF ignition hohlraums can be projected from results achieved to date at a 3.5x smaller scale at Nova and Omega. The more indirect wall-based techniques (thermal and hard x-ray wall imaging) have been useful in providing independent confirmation of ultimately resolved large (e.g. time-averaged ΔP_2 = 15 %) discrepancies between simulated and measured implosion distortions [7, 10]. In this paper, we address the accuracy extrapolated to NIF of the sphere-based symmetry techniques only. We begin by assuming similar spatial resolution and signal-to-noise can be achieved at NIF-scale.

For the re-emission sphere, for fixed hν/4kT ratio, the sensitivity to P_n is then independent of size or temporal scale, hence $\Delta P_2(t) = \pm$ 4 % as reported in Section 2.1. The 2^4x drop in flux by operating at 80 eV instead of the current 160 eV can be fully recovered by noting that the required spatial resolution can scale with hohlraum size and hence re-emission sphere size (e.g. by imaging with 4^2 larger area pinholes).

For the foam ball, the accuracy over any time interval is, by Eq. (1), inversely proportional to the maximum sustainable edge velocity, $\approx 1.5c_s$. Consider a sinusoidal $P_2(\tau)$ variation with period τ. The accuracy in inferring the P_2 amplitude is, rearranging Eq. (1):

$$\Delta P_2 = 2(\sqrt{2}\Delta a_2)(\pi/2)/1.5c_s(\tau/2) \; \approx \; 6\Delta a_2/c_s\tau \qquad (3)$$

where the $\pi/2$ term accounts for the ratio of average to peak P_2, and the $\sqrt{2}$ term accounts for the fact that the difference between two statistically independent measured values of a_n is required to infer a pressure asymmetry. For the foot and peak of the NIF pulse, c_s = 55 and 120 μm/ns. Since Δa_2 = 1 μm from Section 2.2, Eq. (3) yields, for say a 2 ns period, ΔP_2(2 ns) = 5 and 2.5% for the foot and peak of the ignition pulse, respectively. Averaged over a 10 ns foot or 3.5 ns peak pulse, the edge of the foam ball moves ≈ 1/2 of its initial radius, and the time-averaged accuracy is ΔP_2 = 0.5%. For higher order modes, if we assume the same rms measurement accuracy, the accuracy in extracting an a_n coefficient is proportional to $\sqrt{(2n+1)}$. Hence, for a_4, the accuracy is only $\sqrt{9/5} \approx 1.3$x worse than for a_2, in agreement with experimental results. The projected time-averaged ΔP_4 accuracy is then 0.6%.

For the backlit shells, a comparison of Eqs. (1) and (2) shows that the sensitivity over a given distance travelled is intrinsically 2x better than for the foam ball, but only after the shock has transited the shell. The projected asymmetry measurement accuracies for NIF ignition hohlraums are tabulated alongside the ignition requirements in *Fig. 1* by mode number and by technique. *Fig. 1* shows that we have met the measurement requirements for low modes presented in the Section 1. It is implicitly recognized that each of these techniques have or will show the expected sensitivity to intentionally imposed variations in flux asymmetry, as discussed elsewhere [13-16].

4. Time-Resolved Symmetry Experiments at NIF-scale

We have begun demonstrating symmetry techniques at near NIF-scale (2.4-mm-radii hohlraums). The first 6 ns of the NIF hohlraum drive at 80 eV temperatures can be emulated

by Omega and Nova-class lasers. Furthermore, by minimizing P_2 and P_4 asymmetries and taking advantage of increased imaging diagnostic sensitivity at the 3x larger NIF-scale, we hope to demonstrate detection of higher order modes such as P_6 and P_8.

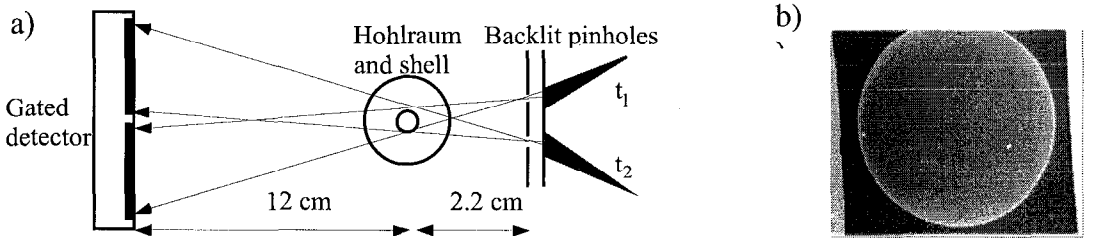

FIG. 2 a) Experimental set-up used at Omega for NIF-scale measurement of flux asymmetry in cylindrical hohlraum. b) Example of 4.7 keV gated backlit image of 14-μm-thick, 3-mm diameter shell driven by a 70 eV, 7 ns drive in a 4.8 by 9 mm long cylindrical hohlraum. Resolution is 30 μm, gate duration is 150 ps.

An example of a NIF-scale experimental set-up for asymmetry diagnosis implemented recently at the Omega facility is shown in *Fig. 2*a. 1.5-3 mm diameter shells or foamballs driven by a 70-80 eV, 7 ns drive in a NIF-size hohlraum are backlit by 4.7 keV x-rays from the He-like Ti 2p-1s resonance transition. Time-resolved backlighting is accomplished by a newly developed technique of backlit pinhole point projection imaging. An example of a gated 30 μm, 150 ps resolution backlit image of a 3-mm-diameter, 14-μm-thick shell consisting of 3% Ge–doped plastic is shown in *Fig.2b*. The limb of the shell is analyzed for distortions induced by flux asymmetries during acceleration, whose radial mid-point vs. polar angle can be determined to much better than the 30 μm resolution. Current results suggest 1-2 μm-accuracy in inferring a_2 distortions is possible, similar to what has been demonstrated at smaller scale and assumed in *Fig. 1*.

*This work was performed under the auspices of the US. Department of Energy by the Lawrence Livermore National Laboratory under contract No. W-7405-ENG-48.

[1] J.D. Lindl, Phys. of Plasmas **2** (1995) 3933.
[2] S.W. Haan, et. al., Phys. of Plasmas **2** (1995) 2480.
[3] O. Jones, et. al., Bull Am. Phys. Soc. (1998).
[4] A.A. Hauer, et. al., Phys. of Plasmas **2** (1995) 2488.
[5] L.J. Suter, et. al., Phys. Rev. Lett. **73** (1994) 2328.
[6] T.J. Murphy, et. al., Phys. of Plasmas **5** (1998) 1960.
[7] N.D. Delamater, et. al., Phys. of Plasmas **3** (1996) 2022.
[8] R.E. Turner, et. al., Phys. of Plasmas, 'in press'.
[9] O.L. Landen, et. al., (these proceedings).
[10] R.L. Kauffman, et. al., Phys. of Plasmas **5** (1998) 1927.
[11] T.J. Murphy, et. al., Phys. Rev. Lett. **82** (1998) 108.
[12] N.D. Delamater, G. R. Magelssen, and A.A. Hauer, Phys. Rev. E **53** (1996) 5240.
[13] G.R. Magelssen, et. al., Phys. Rev. E **57** (1998) 4663.
[14] P.A. Amendt, et. al., Phys. of Plasmas **4** (1997) 1862.
[15] S. G. Glendinning, et. al., Rev. Sci. Instrum. **70** (1999) 536.
[16] O.L. Landen, et. al., Phys. of Plasmas **6** (1999) 2137.
[17] D.H. Kalantar, et. al., Rev. Sci. Instrum. **68** (1997) 814.
[18] M.S. Plesset, J. Appl. Phys. **25** (1954) 96.
[19] W.W. Hsing and N.M. Hoffman, Phys. Rev. Lett. **78** (1997) 3876.